Plant Disease • 2019 • 103:1119-1125 • https://doi.org/10.1094/PDIS-10-18-1778-RE

e-Xtra*

Detection of White Root Rot in Avocado Trees by Remote Sensing

M. L. Pérez-Bueno,[1,†] M. Pineda,[1] C. Vida,[2] D. Fernández-Ortuño,[2] J. A. Torés,[3] A. de Vicente,[2] F. M. Cazorla,[2] and M. Barón[1]

[1]Department of Biochemistry and Molecular and Cellular Biology of Plants, Estación Experimental del Zaidín, Spanish National Research Council (CSIC), Profesor Albareda, 1, 18008, Granada, Spain; [2]Department of Microbiology, Science Faculty of Málaga University, Institute for Mediterranean and Subtropical Horticulture "La Mayora", Málaga University, Spanish National Research Council (IHSM-UMA-CSIC), Boulevard Louis Pasteur, 31, 29071, Málaga, Spain; and [3]Department of Plant Protection, IHSM-UMA-CSIC, Avenue Dr. Wienberg, 29750, Algarrobo-Costa (Málaga), Spain

Abstract

White root rot, caused by the soilborne fungus *Rosellinia necatrix*, is an important constraint to production for a wide range of woody crop plants such as avocado trees. The current methods of detection of white root rot are based on microbial and molecular techniques, and their application at orchard scale is limited. In this study, physiological parameters provided by imaging techniques were analyzed by machine learning methods. Normalized difference vegetation index (NDVI) and normalized canopy temperature (canopy temperature − air temperature) were tested as predictors of disease by several algorithms. Among them, logistic regression analysis (LRA) trained on NDVI data showed the highest sensitivity and lowest rate of false negatives. This algorithm based on NDVI could be a quick and feasible method to detect trees potentially affected by white root rot in avocado orchards.

Keywords: machine learning, NDVI, *Persea americana*, *Rosellinia necatrix*, thermal imaging

Avocado (*Persea americana* Miller) is a highly valued fruit crop in tropical and subtropical regions around the world (Pérez-Jiménez 2008). Spain, the main producer in Europe, is ranked 15th in the world (FAOSTAT 2016). Moreover, 57% of the Spanish avocado area is found in the province of Málaga, in southern Spain, producing 48% of the crop in the country (MAPAMA 2017). In Spain, the most important avocado diseases are Phytophthora root rot, caused by the oomycete *Phytophthora cinnamomi*, and white root rot, caused by the ascomycete fungus *Rosellinia necatrix*. Both diseases are found worldwide but the latter is generally restricted to temperate and subtropical areas such as the Mediterranean basin (Pliego et al. 2009). Indeed, productivity has decreased in southern Spain due to soilborne diseases, and those caused by oomycetes and fungi are the greatest constraints (Pérez-Jiménez 2008).

Avocado trees affected by *R. necatrix* have rotten roots, leading to a water deficit in the aerial part of the plant (Pérez-Jiménez 2006). As a result, leaves show a distinctive yellowing and wilt, and trees eventually die. Evolution of aerial symptoms can occur either quickly (within weeks) or slowly (within years), depending upon environmental, microbial, and plant factors (Guillaumin et al. 1982; Pasini et al. 2016). *R. necatrix* spreads by either mycelial strands growing from infected plants or direct contact between roots from the same or different trees. Thus, white root rot occurs in patches that spread in a circular pattern (Schena et al. 2008).

At present, identification of putative isolates of *R. necatrix* is based on either microscopic observation of the typical pear-shape swellings of its hyphal septa (Eguchi et al. 2009; Petrini 1992; Sztejnberg et al. 1987) or polymerase chain reaction (PCR) analysis (Ruano-Rosa et al. 2007; Schena and Ippolito 2003). Both techniques are time consuming and could delay decisions about possible treatments. Therefore, a quick and economical method for detection and diagnosis of the disease would be desirable.

Remote imaging techniques are widely used in crop protection. Together with information systems, they open new opportunities for precision agriculture (Mahlein 2016; Shakoor et al. 2017). Imaging sensors exploit a wide range of the electromagnetic spectra, and can be used to analyze the effects of biotic or abiotic stress factors on plants (Fiorani and Schurr 2013). Reflectance and thermography are of particular interest in proximal and remote sensing, as well as in plant phenotyping. Reflectance imaging sensors measure light reflected in the visible near-infrared and short-wavelength infrared region of the spectrum (Lowe et al. 2017; Sankaran et al. 2010). Several vegetation indexes can be calculated based on these measurements. For example, the normalized difference vegetation index (NDVI), which estimates vegetation vitality, is broadly used in remote sensing (Pettorelli 2013; Tucker 1979). NDVI has been found to be suitable to distinguish between healthy, asymptomatic, and symptomatic avocado trees affected by laurel wilt (Sankaran et al. 2012). On the other hand, thermography captures radiation in the infrared region of the spectrum. The temperature of the canopy inversely correlates with the leaf transpiration rate, which is controlled by stomatal aperture (Jones 1999). In turn, stomata closure is tightly regulated by plants as a general mechanism of defense upon pathogens and abiotic stress (Melotto et al. 2008). Thus, thermography is widely used to characterize drought susceptibility and response to pests (e.g., pathogens, insects, and nematodes) (Barón et al. 2016; Costa et al. 2013; Mahlein et al. 2012).

The interpretation of images is often challenging and requires integrating knowledge of sensor physics and image analysis. The time-space information collected is large and complex and, consequently, very difficult to analyze by conventional mathematical tools (Fiorani et al. 2012; Pérez-Sanz et al. 2017). The development of advanced statistical methods such as classifiers has been an important contribution to precision agriculture because they enable plant monitoring

†Corresponding author: M. L. Pérez-Bueno;
E-mail: marisa.perez@eez.csic.es

Funding: This work was supported by a grant from Consejería de Economía, Innovación, Ciencia y Empleo, Junta de Andalucía (P12-AGR-0370) to M. Barón, Ministerio de Economía, Industria y Competitividad Consejo Superior de Investigaciones Científicas and European Regional Development Fund (RECUPERA 2020/20134R060) to M. Barón, and Agencia de Innovación y Desarrollo de Andalucía (AGL14-52518-C2-1-R). C. Vida was recipient of a Ph.D. fellowship from the FPI program (MINECO).

*The *e*-**X**tra logo stands for "electronic extra" and indicates that one supplementary appendix is published online.

The author(s) declare no conflict of interest.

Accepted for publication 25 January 2019.

and classification (Behmann et al. 2015). Classifiers have been used to categorize and forecast stressed plants at laboratory (Berdugo et al. 2014; Pérez-Bueno et al. 2016; Pineda et al. 2018), greenhouse (Abdulridha et al. 2016), and field (Calderón et al. 2015; Hou et al. 2016; Sankaran et al. 2013) scales. These algorithms are trained on datasets from different categories or subpopulations. In this way, suitable models would accurately classify new data to the correct category (Singh et al. 2016). Generally, about two-thirds of the dataset is used for training the model while the remaining part is used for validation. Thus, different parameters can be used to evaluate the fit. The most frequent ones are sensitivity, specificity, and accuracy (Ma et al. 2014).

In the present work, NDVI and normalized canopy temperature (canopy temperature [T_c] − air temperature [T_a]) data were collected in an avocado orchard affected by white root rot. Several algorithms, trained on these data, were able to classify trees as healthy or diseased with high accuracy. The suitability of NDVI and temperature of the canopy as predictors is discussed.

Materials and Methods

Study area. This work was conducted in a 1-ha commercial avocado orchard (Hass grafted onto Topa-Topa seedling rootstocks) in Torrox (36°46′05.94″N, 3°56′58.46″W) that contained approximately 300 well-watered trees of different ages. This orchard was particularly suitable for this study because it was distributed in three flat terraces and managed reasonably homogeneously. Irrigation was performed by two sprinklers per tree to ensure an even irrigation across the orchard. Aerial symptoms were estimated for 24 selected trees using the following subjective scale: 0 = healthy or nonsymptomatic, 1 = mild wilt, 2 = severe wilt, and 3 = dead (González-Sánchez et al. 2013).

Fungal detection. The detection on *R. necatrix* and other fungi in roots and surrounding soil was carried out at the time of the measurements in autumn 2015, as previously described by Ruano-Rosa et al. (2007). Soil samples were collected from two points located 1 m from the trunk and on opposite sides of it. The superficial soil was removed in order to localize thick roots with a diameter greater than 5 cm. At each sampling point, three root pieces were obtained and placed in cold storage for transportation to the laboratory. Then, root samples were washed with tap water, and pieces of 0.5 to 1 cm^2 were cut and surface disinfected in a solution of 10% ethanol and 20% sodium hypochlorite for 3 min, then rinsed two times in sterile distilled water. The root samples were then air dried on sterile filter paper for 15 min and placed onto plates of potato dextrose agar (Oxoid Ltd., Hants, UK). The plates were incubated at 25°C for 48 h. Small samples of mycelia growing from roots were collected and grown in individual plates to obtain pure cultures and facilitate their identification.

In order to identify the fungi present in the soil surrounding the trees, avocado twigs (1 to 2 cm in diameter) were inserted into the soil as bait at two diametrically opposed points 0.3 m from the trunk base and 10 to 20 cm deep (Eguchi et al. 2009). After 1 month, the baits were collected and cold stored for transport to laboratory. Fungal isolation from the baits was carried out as described above.

The identification of fungi in pure culture was based on the morphology of its mycelium. To facilitate hyphae observation, preparations of mycelium from each isolate were stained with Amman's lactophenol solution with cotton blue (20 g of phenol, 20 ml of lactic acid, 40 ml of glycerin, 20 ml of distilled water, and 2 ml of cotton blue at 1%). A Nikon Optiphot microscope (Nikon, Tokyo, Japan) equipped with a Moticam Pro 285B camera (Motic Asia, Kowloon, China) controlled by the software Motic Images Plus 2.0 (Motic Asia) was used to observe fungal isolates. *R. necatrix* was identified by the presence of typical pear-shaped swellings near hyphae septa (Petrini 1992; Sivanesan and Holliday 1972).

The detection on *R. necatrix* and other fungi in roots and surrounding soil was carried out at the time of the measurements (in autumn 2015). Furthermore, the presence of *R. necatrix* was corroborated by a PCR-based identification method performed on soil samples collected in 2018. DNA was extracted from 1-g soil samples by a DNeasy PowerSoil Kit (Qiagen N.V. Hilden, Germany) and quantified using a NanoDrop ND-1000 spectrophotometer (Thermo Scientific, Waltham, MA, U.S.A.). The amplification of a 493-bp fragment was performed using the R2 (CAAAACCCATGTGAACATACCA) and R8 (CCGAGGTCAACCTTTGGTATAG) primers (Schena et al. 2002). PCR products were visualized by agarose gel (0.8%) electrophoresis and ethidium bromide staining.

Remotely piloted aircraft system and imaging sensors. In total, eight flights were performed from June through October 2015 (24 June; 1, 8, and 15 July; and 1, 13, 22, and 29 October), providing eight independent replicates. The remotely piloted aircraft system (RPAS) used was the highly portable aerial system DJI S900 (DJI Ltd., Shenzhen, China). Remote control of the RPAS was performed with a computer radio system Futaba 14SG (Hobbico Inc., Champaign, IL, U.S.A.). The software Ground Station (version 3.04; DJI Ltd.) was used to plan the flights, allowing an image overlap of 60 and 75%, horizontally and vertically, respectively.

Three cameras were mounted on the RPAS: (i) a video recording GoPro Hero-3 Silver Edition (GoPro Inc., San Mateo, CA, U.S.A.) with a spatial resolution of 1,920 × 1,080 pixels, (ii) a multispectral reflectance ADC Micro (TetraCam Inc., Chatsworth, Los Angeles, CA, U.S.A.), and (iii) a long-wavelength (7.5 to 13.5 μm) uncooled thermal camera Optris PI-450 (Optris GmbH, Berlin, Germany). The ADC Micro multispectral camera was equipped with three filters atop the sensor that limits the radiation to bands in the green (560 nm), red (660 nm), and near-infrared (830 nm) regions of the spectrum. These bands are equivalent to the Landsat Thematic Mapper bands TM2, TM3, and TM4, respectively. Single images of 2,048 by 1,536 pixels were corrected and used to calculate NDVI images as $(R_{830} - R_{660})/(R_{830} + R_{660})$, according to Tucker (1979). Finally, an NDVI map was built for each time point using the software PixelWrench2 (TetraCam Inc.). The thermal camera Optris PI-450 provided images of 382 by 288 pixels, with a thermal sensitivity of 0.04°C within the range of −20°C to 900°C. Digital video data were recorded and stored in a MiniPC PI Netbox LW (Optris GmbH), also mounted on the RPAS. Air temperature and temperature of two references (black for hottest and white for coldest temperatures) were taken on the field with an Optris MS noncontact infrared thermometer (Optris GmbH). Thermal images were analyzed by software PI Connect (version 2.7.2132.0; Optris GmbH). In this case, only six temperature maps could be obtained.

Image processing and statistical analysis. The software ArcGIS (version 10.4; Esri, Redlands, CA, U.S.A.) was used to compose the mosaic images of the plot using the pictures extracted from the recorded videos. ArcGIS was also used to extract numerical data from thermal and NDVI maps for each individual tree. Moreover, normalized canopy temperature was calculated as difference in canopy and air temperatures ($T_c - T_a$) for each tree. The numerical data were analyzed by Excel 2010 (Microsoft Corporation, Redmond, WA, U.S.A.).

Several classifiers were used to analyze the numerical data (NDVI or NDVI with $T_c - T_a$): artificial neural network (ANN), logistic regression analysis (LRA), linear discriminant analysis (LDA), and support vector machine (SVM) using SPSS (version 23.0; IBM, Armonk, NY, U.S.A.). ANNs, inspired by the biological systems, are one of the most commonly used algorithms (Hahn 2009). Binary LRA is a statistical method widely used in biomedicine because it estimates the probability of a dichotomous outcome ("healthy" versus "infected") (Hosmer et al. 2013). LDA is an algorithm able to find a linear combination of variables that can be used to separate two or more classes of objects (McLachlan 2004). Finally, SVMs represent samples as points in a high-dimensional feature space in which support vectors define a hyperplane that separates samples in classes. SVMs classify new samples based on which side of the hyperplane they fall on (Behmann et al. 2015).

The analysis of NDVI and thermal maps provided two databases. The first one comprised the NDVI values found for each tree in every time point and the second one also contained the $T_c - T_a$ values. Algorithms were trained with 67% of cases in the corresponding database, randomly selected from the numerical database. The remaining

33% of cases in that database were used as validation dataset. Thus, in the case of models fitted with NDVI data (ANN_1 and LRA_1), sample size was 123 in the training set (63 and 60 images from of healthy and diseased trees, respectively) and 61 in the validation set (33 and 28 images from healthy and diseased trees, respectively). For NDVI and $T_c - T_a$ models (ANN_2, LRA_2, LDA, and SVM), sample sizes were 70 (43 for healthy and 33 for diseased) and 40 (22 for healthy and 18 for diseased) in the training and validation set, respectively.

It is worth noting that tree number 11 was asymptomatic but diagnosed as infected in 2015 (Table 1). Therefore, it could not be fit accurately into the defined categories "healthy" or "diseased". Consequently, all data from tree number 11 were excluded from the training dataset used for feeding the algorithms as well as from the subsequent validation datasets.

The goodness of fits were evaluated by the specificity, sensitivity, and accuracy of each model. Sensitivity or true-positive rate is the proportion of infected samples correctly predicted as "infected". Specificity or true-negative rate is the proportion of healthy samples that are correctly identified. Accuracy is the proportion of correct predictions.

Results

White root rot assessment in the orchard. The orchard under study had a previous history of white root rot (Fig. 1A). In June 2015, 24 trees were selected prior to the image analysis. In all, 12 of the selected trees were classified as healthy and 12 as diseased based on aerial symptoms of avocado white root rot and the presence of fungal growth in their roots (Table 1). It is worth noting that most of the trees showing aerial symptoms of white root rot in the orchard (resembling drought stress) were located along the stream (Fig. 1B).

The results of the detection of *R. necatrix* by microbiological diagnoses in root, soil trap, or PCR for the 24 trees under study are summarized in Table 1. The 12 trees diagnosed as healthy were analyzed for the presence of *R. necatrix* in 2015. In nine of them, the pathogen could not be detected by any method. However, the pathogen was found in the surroundings of trees 2, 6, and 12. Nevertheless, the first two trees were still free of pathogen in 2018, while number 12 was found to be infected by PCR diagnosis. In the same way, 12 more trees were analyzed and found positive for the presence of *R. necatrix* in 2015 by at least one of the detection methods. All of them showed aerial symptoms of white root rot, except for tree 11. Thus, tree 11 was classified as level 0 in the scale of symptoms, even though its roots and the surrounding soil contained *R. necatrix*, indicating that this tree was in an early asymptomatic phase of the infection. Consequently, this tree was diagnosed as diseased in 2015 but excluded from the training and validation datasets.

Evaluation of healthy and diseased avocado trees by imaging techniques. Eight measurements of NDVI and six of canopy temperature were carried out from June to October 2015, generating one map per parameter. The average value of NDVI and $T_c - T_a$ was extracted individually for each tree and map.

Trees classified as healthy had significantly higher values of NDVI than those classified as diseased at every measurement ($P < 0.001$; Fig. 2A). Moreover, NDVI was very stable for healthy trees and little or no change was found in the diseased trees during the period of study. Taking into consideration the average NDVI value for trees from all the measurements, a highly significant difference was found between healthy and diseased trees ($P < 0.001$; Fig. 2B and C) and between trees showing symptoms classified as level 1 or 2 of severity ($P < 0.001$ in every case; Fig. 2C). In contrast, the $T_c - T_a$ was higher in diseased trees for every measurement considered independently ($P < 0.1$ and 0.01; Fig. 3A) or all together ($P < 0.001$; Fig. 3B). The $T_c - T_a$ of trees classified as a 1 or 2 on the severity scale showed statistically significant differences relative to the healthy trees ($P < 0.001$ and 0.01, respectively). However, in this case, no significant difference between trees rated as a 1 or 2 was found (Fig. 3C).

Classifying algorithms to identify healthy and diseased avocado trees in the orchard. Several algorithms were fitted to the values of NDVI or $T_c - T_a$ obtained for each avocado tree previously classified as healthy or symptomatic. The features of the used

Table 1. Relation of fungi found in the studied orchard[a]

Tree	Symp[b]	*Rosellinia necatrix* on			Diagnosis[c]	Other fungal genera found in soil
		Roots	Baits	PCR		
1	2	+	–	–	Diseased	*Fusarium, Penicillium, Pythium*
2	0	–	+	–	Healthy	*Fusarium, Aspergillus, Trichoderma, Rhizopus*
3	2	+	+	+	Diseased	*Fusarium, Penicillium, Trichoderma*
4	0	ND	ND	–	Healthy	…
5	1	+	+	–	Diseased	*Fusarium, Aspergillus*
6	0	–	+	–	Healthy	*Fusarium, Aspergillus, Penicillium*
7	1	+	+	+	Diseased	*Fusarium, Aspergillus, Trichoderma*
8	0	ND	ND	–	Healthy	…
9	2	+	–	–	Diseased	*Fusarium, Aspergillus, Trichoderma*
10	0	ND	ND	–	Healthy	…
11	0	+	+	–	Diseased	*Fusarium, Aspergillus*
12	0	–	+	+	Healthy	*Fusarium, Aspergillus, Trichoderma, Penicillium*
13	1	–	+	–	Diseased	*Fusarium, Penicillium*
14	0	ND	ND	–	Healthy	…
15	1	+	+	+	Diseased	*Fusarium, Aspergillus*
16	0	ND	ND	–	Healthy	…
17	2	+	+	–	Diseased	*Fusarium*
18	0	–	–	–	Healthy	*Fusarium, Trichoderma*
19	1	+	+	–	Diseased	*Fusarium, Aspergillus*
20	0	ND	ND	–	Healthy	…
21	2	+	–	–	Diseased	*Fusarium, Trichoderma, Penicillium*
22	0	ND	ND	–	Healthy	…
23	2	+	–	–	Diseased	*Trichoderma, Penicillium*
24	0	ND	ND	–	Healthy	…

[a] Diagnosis of *Rosellinia necatrix* infection on avocado trees based on estimation of aerial symptoms of avocado white root rot and detection of *R. necatrix* in roots and baits (in 2015) and by polymerase chain reaction (PCR) (in 2018).

[b] Aerial symptoms of avocado white root rot: 0 = healthy tree; 1 = light yellowing and wilt in leaves; 2 = yellowing, overall wilt, and some tip leaves dry; and ND = not determined.

[c] Diagnosis in 2015.

classifiers are described in Supplementary Appendix S1. ANN and LRA were the models of choice when only one input variable (either NDVI or $T_c - T_a$) was taken into consideration. According to their sensitivity (79%), specificity (85%), and accuracy (82%), the classification performance of the NDVI models (from now on, ANN_1 and LRA_1) was equivalent (Table 2; Fig. 4). In contrast, $T_c - T_a$ was a bad predictor on its own (e.g., 64% accuracy for LRA; data not shown).

ANN_2, LRA_2, LDA, and SVM were trained on NDVI and $T_c - T_a$ data for each canopy tree at every time point. These four models had the same specificity (86.4%), denoting a good capacity for identifying healthy trees. Conversely, the sensitivity varied from 55.5 for LDA to 78.6% for ANN_2 and SVM, both of them with the highest accuracy (82.5%; Table 2; Fig. 4).

Discussion

Orchards affected by *R. necatrix* usually present a patchy distribution of infected trees. This is mainly because the fungus spreads by dissemination of contaminated materials and from there through the soil by mycelia, and also from tree to tree by mycelial strands along the infected roots in direct contact (Pliego et al. 2009). This orchard was particularly interesting because it was distributed in flat terraces. Moreover, the orchard was known to be efficiently managed, with the orchard manager paying particular attention to the watering schedule and the application of phytosanitary measures in the area under study.

The evaluation of aerial symptoms of avocado white root rot in 2015 delimited the affected area under study. Most of the infected trees were found along the stream line. This is in accordance with previous results showing that soil water content and temperature are the most important factors limiting *R. necatrix* growth (Pasini et al. 2016). The presence of *R. necatrix* in the roots or surrounding soil of symptomatic trees strongly correlated with symptoms of wilting, as previously reported for other crops (Pasini et al. 2016). Moreover, in 2015, this pathogen was found not only in the roots and surrounding soil of diseased trees but also in the soil surrounding healthy trees (numbers 2, 6, and 12). The spreading of *R. necatrix* tree to tree from feeder roots by hyphae (Dann et al. 2013) would explain the presence of the pathogen in the neighborhood of pathogen-free trees and may also be the position of the front line of the fungus spreading through the soil. Nevertheless, the original diagnosis of "healthy" on these three trees in 2015 was confirmed by PCR 3 years later. Furthermore, some typical saprophytic soilborne fungi were detected in soil samples from this orchard (Table 1). However, no correlation was found between their presence and the healthy or symptomatic white root rot status of the trees.

NDVI is widely used to evaluate, among others, plant nitrogen status, chlorophyll content, green leaf biomass, insect infestation, and disease in plants, as reviewed by Pettorelli (2013). In this work, NDVI showed highly significant differences between diseased and healthy avocado trees and between those rated as a 1 or 2 on the scale of symptoms. Moreover, the NDVI values from those trees rated as level 2 showed a tendency to decrease over the course of the study

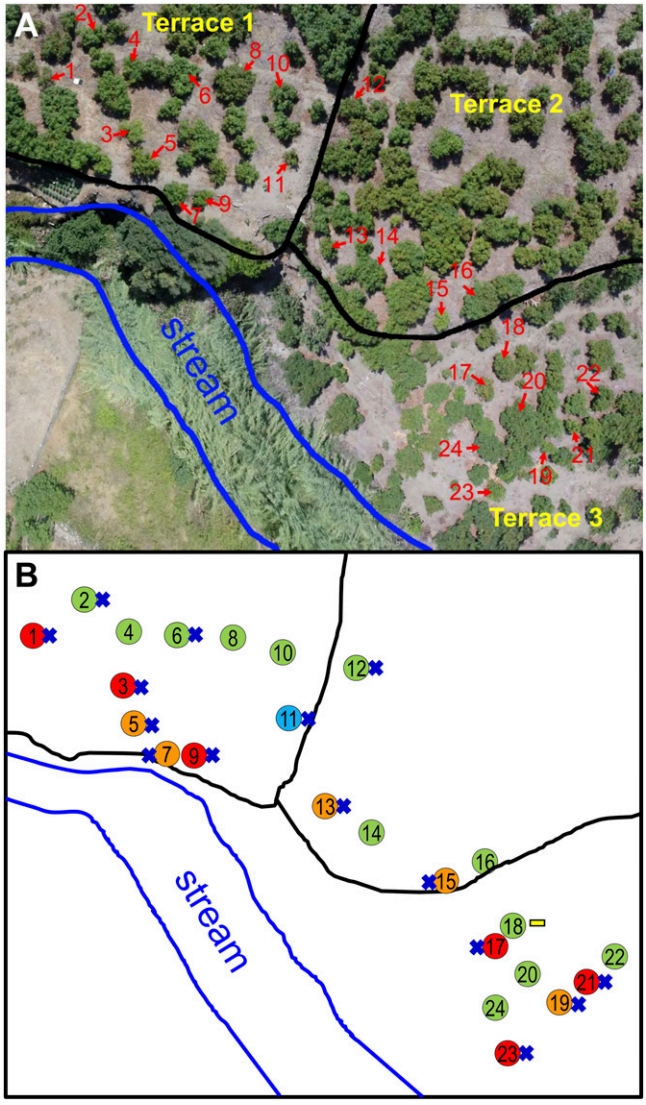

Fig. 1. A, RGB image of the commercial avocado orchard (Hass) located in Torrox. Trees under study are labeled (1 to 24). Terraces and stream within the analyzed area are marked in black and blue, respectively. **B,** Schematic representation of the 2015 disease status of selected trees under study. Each tree is represented by a labeled circle. Colors indicate the scale of aerial symptoms of white root rot in 2015: green for level 0 (asymptomatic trees), orange for level 1 (light yellowing of canopy and mild wilt), and red for level 2 (strong yellowing of the canopy and severe wilt). Blue indicates an asymptomatic tree containing *Rosellinia necatrix* in its roots. For each tree, a blue cross indicates positive detection of *R. necatrix* in root or bait samples and the yellow bar indicates negative detection of *R. necatrix*, according to the analyses carried out on 2015 samples.

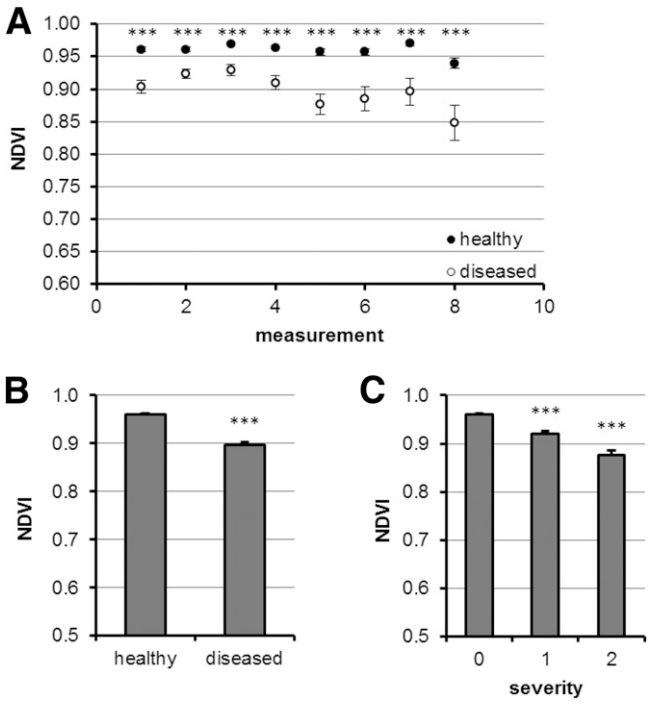

Fig. 2. A, Mean normalized difference vegetation index (NDVI) values for healthy and diseased trees for each measuring time. **B,** Mean NDVI values for healthy and diseased trees averaged for all measuring times. **C,** Mean NDVI values for healthy trees and trees classified as level 1 or 2 in the scale of symptoms averaged for all measuring times. Error bars indicate standard error and *** denotes $P < 0.001$, according to a one-way analysis of variance (ANOVA) test (A and B) or one-way ANOVA with honestly significant difference Tukey post hoc test (C). Asymptomatic tree number 11 was excluded from this analysis.

(data not shown). This decrease in NDVI could be related to a decrease in the chlorophyll content, as previously reported for avocado trees affected by *Raffaelea lauricola*, which causes symptoms similar to those of white root rot (Sankaran et al. 2012). Unlike NDVI, the $T_c - T_a$ did not show a clear ability to discriminate between healthy and diseased trees in this study. These findings are in accordance with a previous work suggesting that severe metabolic changes in *Rosellinia necatrix*-infected avocado trees, including those related to leaf temperature, only take place at late stages of the infection. Those metabolic changes were suggested to be related to the loss of functionality of the plant radical system (Granum et al. 2015).

Several authors have addressed the identification of infected plants by analyzing reflectance indices. For example, the infection by *R. lauricola* has been analyzed by a nonimaging spectroradiometer on detached leaves of avocado trees growing in greenhouses. Class accuracies were 56 and 100% for very mild and severe symptoms, respectively (Abdulridha et al. 2016; Sankaran et al. 2012). Similarly, de Castro et al. (2015) defined the parameter ExR (based on RGB images), which offered the best contrast between laurel wilt-affected and healthy trees. However, no information about sensitivity, specificity, or accuracy was provided. On the other hand, grapevines suffering from grapevine leafroll disease could be identified at different stages of the disease. In that case, NDVI and other multispectral parameters were analyzed by an ant colony clustering algorithm with class accuracies ranging from 75 to 94.4%, depending on the severity of symptoms (Hou et al. 2016). Reflectance measurements have also been used to study the bacterial disease huanglongbing or citrus greening in citrus groves. Measurements obtained with a multiband and hyperspectral camera achieved 67 to 85% accuracy with a 7 to 32% false-negative rate by applying an SVM to the multiband images (García-Ruíz et al. 2013). In addition, Yang et al. (2010) used multiband and hyperspectral cameras to study cotton root rot caused by the fungus *Phymatotrichum omnivorum*. These authors used principal component analysis to obtain an overall accuracy of 96 to 98% when classifying root-rot-infested and noninfested areas. More recently, NDVI combined with unsupervised classification was shown to be an effective tool for detecting cotton root rot, reaching overall accuracy values of up to 95% when using an aircraft-based multispectral camera (Yang et al. 2015) or historical satellite images (Yuan et al. 2016).

Reflectance imaging has been combined with thermography for the analysis of healthy and diseased trees. That was the case in the study by Calderón et al. (2015), in which olive trees infected by *Verticillium dahliae* were analyzed by an SVM on temperature and vegetation indices, reaching an overall accuracy of 79%. However, LDA classified trees at low severity levels, obtaining a better class accuracy than SVM (75 and 40.6%, respectively). In a study on citrus greening, a number of classifying models were applied to several spectral bands plus thermal data (Sankaran et al. 2013). Among those models, SVM provided the best performance, with an overall accuracy of 87% and the lowest rate of false negatives. However, in the present work, the use of thermal data as an input feature for classifiers did not improve substantially the accuracy of the algorithms trained on an NDVI database. Thus, accuracy and specificity were slightly higher for ANN_2 and SVM than for ANN_1 and LRA_1. However, ANN_1 and LRA_1 had higher sensitivity and, consequently, a lower

Table 2. Confusion matrices for the validation of the models artificial neural network $(ANN)_1$ and logistic regression analysis $(LRA)_1$ (normalized difference vegetation index [NDVI] as the only input feature) and ANN_2, LRA_2, lineal discriminant analysis (LDA), and support vector machine (SVM) (NDVI and normalized canopy temperature as input features)

		Predicted	
Algorithm	**Observed**	**Healthy**	**Diseased**
ANN_1	Healthy	28	5
	Diseased	6	22
LRA_1	Healthy	28	5
	Diseased	6	22
ANN_2	Healthy	19	3
	Diseased	4	14
LRA_2	Healthy	19	3
	Diseased	5	13
LDA	Healthy	19	3
	Diseased	8	10
SVM	Healthy	19	3
	Diseased	4	14

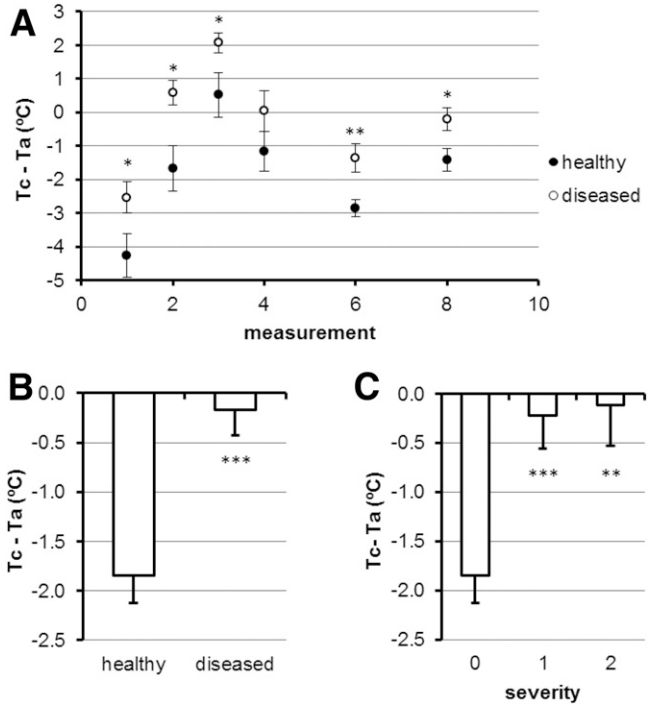

Fig. 3. A, Mean normalized canopy temperature (canopy temperature [T_c] – air temperature [T_a]) for healthy and diseased trees for each measuring time. **B,** Mean $T_c - T_a$ values for healthy and diseased trees averaged for all measuring times. **C,** Mean $T_c - T_a$ values for healthy trees and trees classified as level 1 or 2 in the scale of symptoms averaged for all measuring times. Error bars indicate standard error; *, **, and *** indicate $P < 0.1$, 0.01, and 0.001, respectively, according to the one-way analysis of variance (ANOVA) test (A and B) or one-way ANOVA with honestly significant difference Tukey post hoc test (C). Asymptomatic tree number 11 was excluded from this analysis.

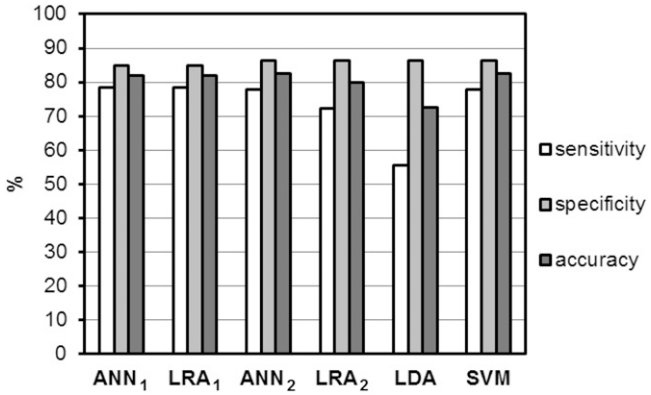

Fig. 4. Values of sensitivity, specificity, and accuracy evaluating the goodness of the performance of the best models trained on normalized difference vegetation index (NDVI) data or NDVI and canopy temperature – air temperature: artificial neural network (ANN), logistic regression analysis (LRA), lineal discriminant analysis (LDA), and support vector machine (SVM). Sensitivity and specificity are the true positive and negative rate, respectively, and accuracy is the rate of true results over the number of cases analyzed.

false-negative rate, in which case these algorithms could be considered the most appropriate method for disease detection (Sankaran et al. 2013).

The current methods of detection of *R. necatrix*, based on microbial and molecular techniques, have serious limitations for their application in large orchards. For example, tree number 13 was diagnosed to be infected by *R. necatrix* according to its symptoms, whereas all of the analysis performed in 2015 on roots and soil were negative for the presence of pathogens. In addition, infected trees can go undetected until the appearance of aerial symptoms. These issues make the detection of the pathogen across large areas extremely difficult. Consequently, rapid, reliable, sensitive, inexpensive, and easy-to-use diagnostic methods for fungal pathogen detection would be desirable (Ray et al. 2017). Remote sensing appears to be a suitable approach to study the progress of infections and the control of this pathogen in crop fields because they provide sensitivity and promptness and are cost effective. However, the development of diagnostic methods based on imaging techniques faces the challenge of identifying asymptomatic or weakly symptomatic individuals. Indeed, the literature is replete with examples where it was concluded that classification of diseased trees at early stages of infection by imaging-based methods is very difficult (Abdulridha et al. 2016; Calderón et al. 2015; Hou et al. 2016; Leckie et al. 2004; Sankaran et al. 2012). The performance of the classifying algorithms based on NDVI reported here for *R. necatrix*-infected avocado trees is comparable with the results found in the literature, suggesting the method to be suitable for the detection of diseased avocado trees in the field.

The use of NDVI recorded from an RPAS as the only input feature for an ANN or LRA appears to be a reliable and inexpensive method to detect avocado trees potentially affected by white root rot, even when the symptoms are very mild or absent. However, the disease could be due to multiple causes that are not specific to this disease. Consequently, the remote sensing methods could be used as a quick "prescreening" procedure to identify potentially diseased trees. LRA_1 was the most reliable classifier because it showed the best general performance, with the highest sensitivity and lowest rate of false negatives. Furthermore, LRA_1 is only based on data obtained by a multispectral camera, providing a simple detection method. This methodology could be particularly relevant in southern Spain, the largest producer of avocado in Europe, where production has been particularly threatened in recent years due to white root rot.

Acknowledgments

This article is dedicated to the memory of Dr. Juan Antonio Torés (1952–2018). We thank F. M. Cabeza for assistance in relation to the acquisition of multispectral and thermal images.

Literature Cited

Abdulridha, J., Ehsani, R., and de Castro, A. 2016. Detection and differentiation between laurel wilt disease, phytophthora disease, and salinity damage using a hyperspectral sensing technique. Agriculture 6:56.

Barón, M., Pineda, M., and Pérez-Bueno, M. L. 2016. Picturing pathogen infection in plants. Z. Naturforsch. C Biol. Sci. 71:355-368.

Behmann, J., Mahlein, A.-K., Rumpf, T., Römer, C., and Plümer, L. 2015. A review of advanced machine learning methods for the detection of biotic stress in precision crop protection. Precis. Agric. 16:239-260.

Berdugo, C. A., Zito, R., Paulus, S., and Mahlein, A. K. 2014. Fusion of sensor data for the detection and differentiation of plant diseases in cucumber. Plant Pathol. 63:1344-1356.

Calderón, R., Navas-Cortés, J. A., and Zarco-Tejada, P. J. 2015. Early detection and quantification of Verticillium wilt in olive using hyperspectral and thermal imagery over large areas. Remote Sens. Environ. 7:5584-5610.

Costa, J. M., Grant, O. M., and Chaves, M. M. 2013. Thermography to explore plant–environment interactions. J. Exp. Bot. 64:3937-3949.

Dann, E. K., Ploetz, R. C., Coates, L. M., and Pegg, K. G. 2013. Foliar, fruit and soilborne diseases. Pages 380-422 in: The Avocado: Botany, Production and Uses. A. Schaffer, N. Wolstenholme, and A. W. Whiley, eds. CAB International, Wallingford, UK.

de Castro, A. I., Ehsani, R., Ploetz, R. C., Crane, J. H., and Buchanon, S. 2015. Detection of laurel wilt disease in avocado using low altitude aerial imaging. PLoS One 10:e0124642.

Eguchi, N., Kondo, K.-i., and Yamagishi, N. 2009. Bait twig method for soil detection of *Rosellinia necatrix*, causal agent of white root rot of Japanese pear and apple, at an early stage of tree infection. J. Gen. Plant Pathol. 75:325-330.

FAOSTAT. 2016. Ranking of countries by commodity: Avocados. www.fao.org/faostat/en/#rankings/countries_by_commodity

Fiorani, F., Rascher, U., Jahnke, S., and Schurr, U. 2012. Imaging plants dynamics in heterogenic environments. Curr. Opin. Biotechnol. 23:227-235.

Fiorani, F., and Schurr, U. 2013. Future scenarios for plant phenotyping. Annu. Rev. Plant Biol. 64:267-291.

García-Ruíz, F., Sankaran, S., Maja, J. M., Lee, W. S., Rasmussen, J., and Ehsani, R. 2013. Comparison of two aerial imaging platforms for identification of Huanglongbing-infected citrus trees. Comput. Electron. Agric. 91:106-115.

González-Sánchez, M. Á., de Vicente, A., Pérez-García, A., Pérez-Jiménez, R., Romero, D., and Cazorla, F. M. 2013. Evaluation of the effectiveness of biocontrol bacteria against avocado white root rot occurring under commercial greenhouse plant production conditions. Biol. Control 67:94-100.

Granum, E., Pérez-Bueno, M. L., Calderón, C. E., Ramos, C., de Vicente, A., Cazorla, F. M., and Barón, M. 2015. Metabolic responses of avocado plants to stress induced by *Rosellinia necatrix* analysed by fluorescence and thermal imaging. Eur. J. Plant Pathol. 142:625-632.

Guillaumin, J. J., Mercier, S., and Dubos, B. 1982. Les pourridiés à *Armillariella* et *Rosellinia* en France sur vigne, arbres fruitiers et cultures florales I. Etiologie et symptomatologie. Agronomie 2:71-80.

Hahn, F. 2009. Actual pathogen detection: Sensors and algorithms—A review. Algorithms 2:301-338.

Hosmer, J., David, W., Lemeshow, S., and Sturdivant, R. X. 2013. Applied Logistic Regression, 3rd ed. John Wiley & Sons, Inc., Hoboken, NJ, U.S.A.

Hou, J., Li, L., and He, J. 2016. Detection of grapevine leafroll disease based on 11-index imagery and ant colony clustering algorithm. Precis. Agric. 17: 488-505.

Jones, H. G. 1999. Use of thermography for quantitative studies of spatial and temporal variation of stomatal conductance over leaf surfaces. Plant Cell Environ. 22:1043-1055.

Leckie, D. G., Jay, C., Gougeon, F. A., Sturrock, R. N., and Paradine, D. 2004. Detection and assessment of trees with *Phellinus weirii* (laminated root rot) using high resolution multi-spectral imagery. Int. J. Remote Sens. 25:793-818.

Lowe, A., Harrison, N., and French, A. P. 2017. Hyperspectral image analysis techniques for the detection and classification of the early onset of plant disease and stress. Plant Methods 13:80.

Ma, C., Zhang, H. H., and Wang, X. 2014. Machine learning for big data analytics in plants. Trends Plant Sci. 19:798-808.

Mahlein, A.-K. 2016. Plant disease detection by imaging sensors—Parallels and specific demands for precision agriculture and plant phenotyping. Plant Dis. 100:241-251.

Mahlein, A. K., Oerke, E. C., Steiner, U., and Dehne, H. W. 2012. Recent advances in sensing plant diseases for precision crop protection. Eur. J. Plant Pathol. 133: 197-209.

MAPAMA. 2017. Datos avances de frutales no cítricos y frutales secos año 2017. https://www.mapama.gob.es/es/estadistica/temas/estadisticas-agrarias/agricultura/superficies-producciones-anuales-cultivos

McLachlan, A. 2004. Discriminant Analysis and Statistical Pattern Recognition. John Wiley & Sons, Inc., Hoboken, NJ, U.S.A.

Melotto, M., Underwood, W., and He, S. Y. 2008. Role of stomata in plant innate immunity and foliar bacterial diseases. Annu. Rev. Phytopathol. 46:101-122.

Pasini, L., Prodorutti, D., Pastorelli, S., and Pertot, I. 2016. Genetic diversity and biocontrol of *Rosellinia necatrix* infecting apple in northern Italy. Plant Dis. 100:444-452.

Pérez-Bueno, M. L., Pineda, M., Cabeza, F., and Barón Ayala, M. 2016. Multicolor fluorescence imaging as a candidate for disease detection in plant phenotyping. Front. Plant Sci. 7:1790.

Pérez-Jiménez, R. M. 2006. A review of the biology and pathogenicity of *Rosellinia necatrix*—The cause of white root rot disease of fruit trees and other plants. J. Phytopathol. 154:257-266.

Pérez-Jiménez, R. M. 2008. Significant avocado diseases caused by fungi and oomycetes. Eur. J. Plant Sci. Biotechnol. 2:1-24.

Pérez-Sanz, F., Navarro, P. J., and Egea-Cortines, M. 2017. Plant phenomics: An overview of image acquisition technologies and image data analysis algorithms. Gigascience 6:1-18.

Petrini, L. E. 1992. *Rosellinia* species of the temperate zones. Sydowia 44: 169-281.

Pettorelli, N. 2013. The Normalized Difference Vegetation Index. Oxford University Press, Oxford, United Kingdom.

Pineda, M., Pérez-Bueno, M. L., and Barón, M. 2018. Detection of bacterial infection in melon plants by classification methods based on imaging data. Front. Plant Sci. 9:164.

Pliego, C., Kanematsu, S., Ruano-Rosa, D., de Vicente, A., López-Herrera, C., Cazorla, F. M., and Ramos, C. 2009. GFP sheds light on the infection process of avocado roots by *Rosellinia necatrix*. Fungal Genet. Biol. 46: 137-145.

Ray, M., Ray, A., Dash, S., Mishra, A., Achary, K. G., Nayak, S., and Singh, S. 2017. Fungal disease detection in plants: Traditional assays, novel diagnostic techniques and biosensors. Biosens. Bioelectron. 87:708-723.

Ruano-Rosa, D., Schena, L., Ippolito, A., and López-Herrera, C. J. 2007. Comparison of conventional and molecular methods for the detection of *Rosellinia necatrix* in avocado orchards in southern Spain. Plant Pathol. 56: 251-256.

Sankaran, S., Ehsani, R., Inch, S. A., and Ploetz, R. C. 2012. Evaluation of visible-near infrared reflectance spectra of avocado leaves as a non-destructive sensing tool for detection of laurel wilt. Plant Dis. 96:1683-1689.

Sankaran, S., Maja, J. M., Buchanon, S., and Ehsani, R. 2013. Huanglongbing (citrus greening) detection using visible, near infrared and thermal imaging techniques. Sensors (Basel) 13:2117-2130.

Sankaran, S., Mishra, A., Ehsani, R., and Davis, C. 2010. A review of advanced techniques for detecting plant diseases. Comput. Electron. Agric. 72:1-13.

Schena, L., and Ippolito, A. 2003. Rapid and sensitive detection of *Rosellinia necatrix* in roots and soils by real time Scorpion-PCR. J. Plant Pathol. 85:15-25.

Schena, L., Nigro, F., and Ippolito, A. 2002. Identification and detection of *Rosellinia necatrix* by conventional and real-time Scorpion-PCR. Eur. J. Plant Pathol. 108:355-366.

Schena, L., Nigro, F., and Ippolito, A. 2008. Integrated management of *Rosellinia necatrix* root rot on fruit tree crops. Pages 137-158 in: Integrated Management of Diseases Caused by Fungi, Phytoplasma and Bacteria, Vol. 3. A. Ciancio and K. G. Mukerji, eds. Springer, Dordrecht, The Netherlands.

Shakoor, N., Lee, S., and Mockler, T. C. 2017. High throughput phenotyping to accelerate crop breeding and monitoring of diseases in the field. Curr. Opin. Plant Biol. 38:184-192.

Singh, A., Ganapathysubramanian, B., Singh, A. K., and Sarkar, S. 2016. Machine learning for high-throughput stress phenotyping in plants. Trends Plant Sci. 21: 110-124.

Sivanesan, A., and Holliday, P. 1972. *Rosellinia necatrix*. CMI Descr. Pathog. Fungi Bacteria 352:1-2.

Sztejnberg, A., Freeman, S., Chet, I., and Katan, J. 1987. Control of *Rosellinia necatrix* in soil and in apple orchard by solarization and *Trichoderma harzianum*. Plant Dis. 71:365-369.

Tucker, C. J. 1979. Red and photographic infrared linear combinations for monitoring vegetation. Remote Sens. Environ. 8:127-150.

Yang, C., Everitt, J. H., and Fernandez, C. J. 2010. Comparison of airborne multispectral and hyperspectral imagery for mapping cotton root rot. Biosyst. Eng. 107:131-139.

Yang, C., Odvody, G. N., Fernandez, C. J., Landivar, J. A., Minzenmayer, R. R., and Nichols, R. L. 2015. Evaluating unsupervised and supervised image classification methods for mapping cotton root rot. Precis. Agric. 16:201-215.

Yuan, L., Pu, R., Zhang, J., Wang, J., and Yang, H. 2016. Using high spatial resolution satellite imagery for mapping powdery mildew at a regional scale. Precis. Agric. 17:332-348.